Novel inhibitory compositions based on 4,5,6,7-tetrahydro-[1,2,4]triazolo[1,5-*a*]pyrimidin-7-ol derivatives for steel acid corrosion protection

A.A. Kruzhilin,[1] D.S. Shevtsov,[1] A.Yu. Potapov,[1] Kh.S. Shikhaliev,[1]* O.A. Kozaderov,[1] Ch. Prabhakar[2] and V.E. Kasatkin[3]

[1]Voronezh State University, 1 Universitetskaya pl., 394018 Voronezh, Russian Federation
[2]National Institute of Technology Kurukshetra, 136119 Kurukshetra, India
[3]A.N. Frumkin Institute of Physical Chemistry and Electrochemistry, Russian Academy of Sciences, Leninsky pr. 31, 119071 Moscow, Russian Federation
**E-mail: shikh1961@yandex.ru*

Abstract

The inhibitive effect of several synthesized derivatives of the 1,2,4-triazole class on St3 steel corrosion in 24% HCl solution is revealed. The derivatives consist of 3-alkyl-5-amino-1*H*-1,2,4-triazoles obtained from a mixture of fatty acids – coconut oil processing waste, individual 2-methyl-5-phenyl-4,5,6,7-tetrahydro-[1,2,4]triazolo[1,5-*a*]pyrimidin-7-ol, as well as two compositions based on these triazoles, cinnamaldehyde and surfactant. The structure of the synthesized compounds was proved using NMR spectroscopy and HPLC/MS spectrometry. Different electrochemical and physical methods were used to determine the high protective effect of the studied derivatives at concentration (C_{inh}) from 0.10 to 2.00 g·dm^{-3}. The SEM microphotographs of the steel surface after exposure in HCl solutions without additives and in the presence of the studied substances and compositions allowed us to visually evaluate the inhibition effectiveness of the obtained compounds. Quantum-chemical calculations were carried out using the density functional theory (DFT), as a result, the correlation between the protective properties and the electronic structure of the molecules of the studied compounds was found and substantiated. It has been established that the developed compositions of inhibitors, as well as 2-methyl-5-phenyl-4,5,6,7-tetrahydro-[1,2,4]triazolo[1,5-*a*]pyrimidin-7-ol, have a significant anticorrosive effect. Optimum results were obtained when inhibitor compositions were used: the protection degree for them was more than 95% at an inhibitor concentration of at least 0.50 g·dm^{-3}, while the corrosion rate was 0.4–1.0 g/m^2·hour. The high protective effect of the developed compositions is probably associated with the reaction of aminotriazoles with cinnamaldehyde during the preparation of the inhibitory compositions. This reaction results in the formation of the corresponding derivatives of the 2-alkyl-5-phenyl-4,5,6,7-tetrahydro-[1,2,4]triazolo[1,5-*a*]pyrimidin-7-ol class, similarly to the formation of 2-methyl-5-phenyl-4,5,6,7-tetrahydro-[1,2,4]triazolo[1,5-*a*]pyrimidin-7-ol that we synthesized intentionally.

Received: May 28, 2022. Published: June 8, 2022 doi: 10.17675/2305-6894-2022-11-2-22

Keywords: *corrosion, steel, inhibitors, heterocyclic compounds, aminotriazoles, tetrahydrotriazolopyrimidinols, electrochemical impedance spectrometry, potentiodynamic polarization, scanning electron microscopy, drilling equipment, vegetable oil, chemical processing of organic waste.*

1. Introduction

Acid treatments of oil and gas wells are typically used to create artificial channels in carbonate formations and to increase their permeability by dissolving clays and other materials that clog pores near the wellbore. Acetic acid, hydrochloric acid, or a mixture of hydrofluoric and hydrochloric acids are usually used as acids injected into the reservoir through wells [1].

Since these solutions can cause severe corrosion of both casing and coiled tubing strings, this treatment requires the use of so-called inhibited acids obtained by adding corrosion inhibitors to the aforementioned acid solutions. Inhibitor films generally protect bare metal from corrosion by creating a "barrier" between the aggressive acid solution and the metal surface. Nowadays a wide range of organic film-forming corrosion inhibitors is known [2].

At the moment, the most studied group of organic substances that exhibit an anticorrosive effect on steel includes numerous nitrogen and sulfur-containing heterocyclic compounds, for instance, aminopyrazoles [3], aminopyridines [4], pyrimidines [5, 6], thiazoles [7], benzimidazoles [8, 9], *etc.* However, the undoubted and undeniable leaders in this segment are the triazole derivatives. In particular, the action of benzotriazole (BTA) has been studied in detail in relation to ferrous and non-ferrous metals [10–12]. This substance is considered as a universal inhibitor for various media, but it has several disadvantages. Its degree of protection and steel acid corrosion inhibition coefficients are not very high. It is also known to be moderately hepatotoxic, mutagenic, and its semi-lethal dose is rather low (LD50 ~ 560 mg/kg [13]). In this regard, in recent years, a trend to search for new environmentally friendly, non-toxic, and effective corrosion inhibitors has been formed.

Fatty acids, which are mostly environmentally friendly, biodegradable compounds involved in the metabolism of many organisms, can be used to obtain a variety of organic compounds, including corrosion inhibitors for both ferrous and non-ferrous metals. For example, fatty acid hydrazides and thiosemicarbazides [14] or Schiff bases of soybean oil fatty acids [15] inhibit steel corrosion. Heterocyclic steel corrosion inhibitors synthesized from carboxylic acids are known, such as imidazoles [16] or 3-alkyl-5-mercapto-1,2,4-triazoles [17]. At the same time, amitrol, the simplest representative of the aminotriazole class, is slightly toxic (LD50 = 1100 mg/kg). [18].

In this regard, an important and urgent task is the synthesis of new effective heterocyclic inhibitors of the 1,2,4-triazole class, including those based on vegetable oil processing products, in order to study their properties against steel corrosion in acidic media. The aim of this work was to study the anticorrosive activity of 3-alkyl-5-amino-1*H*-1,2,4-triazole

derivatives and 5-phenyl-4,5,6,7-tetrahydro-1,2,4]triazolo[1,5-*a*]pyrimidin-7-ol derivatives under conditions of mild steel corrosion in hydrochloric acid.

2. Experimental

2.1. Methods for analyzing the chemical structure and composition of inhibitors

Gas chromatographic mass spectrometric analysis (GC-MS) was performed using an Agilent Technologies 7890B GC system with an Agilent Technologies 5977A MSD mass selective detector. Before analysis, the fatty acids were converted to the corresponding methyl esters. To do this, the fatty acids were boiled in methanol with a catalytic amount of sulfuric acid and extracted three times with hexane. The resulting extract was evaporated. A weighed portion of FAMEs was dissolved in 10 ml of hexane. An internal standard (ethyl butyrate) with a known concentration was added, and the mixture was analyzed.

Aminotriazoles were analyzed by high performance liquid chromatography with high resolution mass spectrometric detection using electrospray ionization (HPLC-HRMS-ESI) combined with UV detection. The device consisted of an Agilent 1269 Infinity liquid chromatograph and an Agilent 6230 TOF LC/MS high-resolution time-of-flight mass detector. Quantitative determination was performed by the internal standard method.

^{1}H NMR spectra were recorded on a Bruker AV600 spectrometer (600.13 MHz) in DMSO-d6, TMS was the internal standard. The acid number of the products was determined by titrimetric analysis as described in GOST R. EN. 14104-2009. “Derivatives of fats and oils // Methyl esters of fatty acids (FAME). Determination of acid number”.

Coconut oil processing waste was a mixture of coconut oil fatty acids and was provided by EFKO Group of Companies (Alekseevka, Belgorod region, Russian Federation) (acid value is 193.9 mg·KOH/g), the composition of the mixture according to GC/MS analysis is presented in Table 1. Other reagents were purchased from Acros Organics.

Table 1. The composition of coconut oil fatty acid mixture.

Fatty acid	Content, %
C6	21.5
C8	9.4
C10	37.5
C12	6.9
C14	7.3
C16	5.6
C18:1 (9)	2.5
Other	~9.3

2.2. Synthesis and analysis of inhibitors

The mixture of aminotriazoles of coconut acids (ATCA) was investigated as a novel inhibitory composition for steel acid corrosion protection. The general formula of these aminotriazoles is shown in Figure 1:

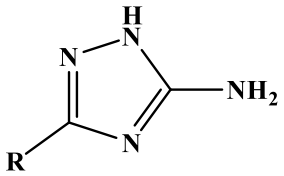

Figure 1. General formula of aminotriazoles in ATCA mixture.

ATCA was synthesized from a coconut oil processing waste, which is a mixture of fatty acids, according to the previously described method [19].

The composition of ATCA according to GC-MS and HPLC-MS analysis is presented in Table 2. Acid number was 38.5 mg·KOH/g. The yield was 95%. ^{1}H-NMR (DMSO-d6 δ (ppm): 0.83–0.90 ($CH_{3(alkyl)}$+$CH_{3(butyl)}$), 1.23–1.34 ($CH_{2(alkyl)}$+$CH_{2(butyl)}$), 1.43–1.56 (β$CH_{2(alkyl)}$), 1.96–2.08 ($CH_2CH{=}CH_{(alkyl)}$), 2.26–2.39 (α$CH_{2(alkyl)}$+β$CH_{2(butyl)}$), 2.72–2.75 ($CH{=}CHCH_2CH{=}CH_{(alkyl)}$), 3.98–4.01 (α$CH_{2(butyl)}$), 5.27–5.37 ($CH{=}CH_{(alkyl)}$), 5.44 ($NH_2$), 11.80 (NH).

The resulting ATCA mixture contains 75.4% 3-alkyl-5-amino-1*H*-1,2,4-triazoles and in addition 16.6% fatty acids and their butyl esters (Table 2), because the process is accompanied by esterification of fatty acids with butanol, which was the solvent in the reaction. Further investigation of the obtained product was carried out without additional purification.

Table 2. The composition of the ATCA aminotriazole mixture based on coconut oil processing waste.

Fatty acid	Fatty acid content in the oil waste, %	Aminotriazoles content in the product, %	Butyl ethers content in the product, %
C6	21.5	19.9	3.2
C8	9.4	5.8	4.5
C10	37.5	33.7	3.0
C12	6.9	4.9	2.7
C14	7.3	5.2	1.6
C16	5.6	4.2	1.0
C18:1 (9)	2.5	1.7	0.6
Total	100	75.4	16.6

We also synthesized 2-methyl-5-phenyl-4,5,6,7-tetrahydro-[1,2,4]triazolo[1,5-*a*]pyrimidin-7-ol (MPTTP) by the reaction of 3-methyl-5-amino-1,2,4-triazole with cinnamaldehyde (Figure 2). Later, this compound was also investigated as an inhibitor of steel corrosion in an acidic solution.

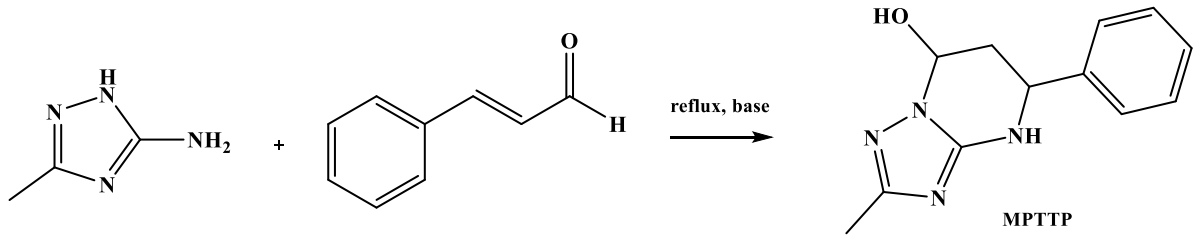

Figure 2. Scheme for the synthesis of 2-methyl-5-phenyl-4,5,6,7-tetrahydro-[1,2,4]triazolo[1,5-*a*]pyrimidin-7-ol.

A mixture of 1 mole of 3-methyl-5-amino-1*H*-1,2,4-triazole and 2 moles of cinnamaldehyde in 100 ml of morpholine was refluxed for 3 hours. Then the solvent was removed, the residue was recrystallized from isopropanol and washed with diethyl ether. The product yield was 65–70%.

The structure of MPTTP obtained was confirmed by ^{1}H NMR and HPLC/MS. ^{1}H NMR (DMSO-d_6), δ (ppm): 2.05–2.10 (s, CH_3, 3H), 2.30–2.38 (m, CH–Ph, 1H), 2.75–2.85 (m, CH–OH, 1H), 3.05–3.10 (m, CH–Ph, 1H), 3.48-3.60 (m, CH_2, 2H), 3.85–3.95 (m, CH–Ph, 1H), 4.40–4.70 (m, CH–OH, 1H), 4.95–5.05 (br.s, OH, 1H), 7.05–7.10 (br.s, NH), 7.20–7.50 (m, aromatic, 5H).

An inhibitory composition IC1 was obtained by mixing equal weight parts of ATCA, cinnamaldehyde and an aqueous solution of cocamidopropyl betaine (40%). All the components were mixed with constant stirring and slight heating (60–70°C) and then cooled and used in further anticorrosive investigations.

HPLC/MS analysis of the IC1 composition obtained gave unexpected results. The main components of the mixture were derivatives of tetrahydro- and dihydro-[1,2,4]triazolo[1,5-*a*]pyrimidin-7-ols of the general formula shown in Figure 3. The results of quantitative analysis of IC1 composition are presented in Table 3.

The inhibitory composition IC2 was prepared similarly to IC1 composition.

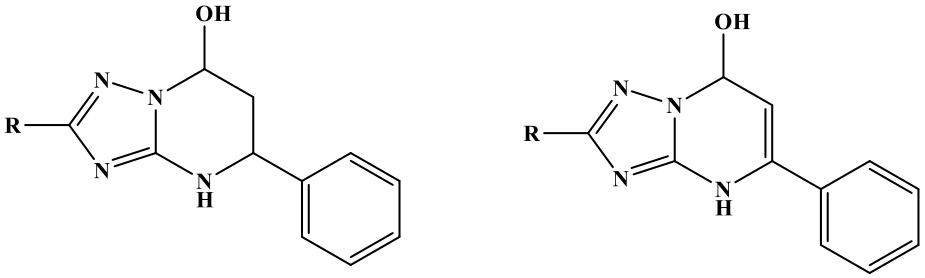

Figure 3. Structures of tetrahydro- and dihydro-[1,2,4]triazolo[1,5-*a*]pyrimidin-7-ols in IC1 composition.

Table 3. The content of the main components of IC1 composition based on HPLC/MS data.

Mass fraction of the component, %	**3.84**	**5.83**	**19.93**	**36.55**	**3.65**	**6.18**	**6.68**	**4.33**	**2.02**
Component, *R*=	C6	C8	C6 (dihydro)	C10	C8 (dihydro)	C12	C14	C16	C18:1 (dihydro)

A mixture of equal weight parts of 3-methyl-5-amino-1*H*-1,2,4-triazole, cinnamaldehyde and an aqueous solution of cocamidopropyl betaine (40%) was kept under constant stirring and at a temperature of 60–70°C for 2–3 minutes until obtaining a homogeneous paste-like substance. Cooling the resulting mass led to the formation of a white crystalline powder of IC2.

HPLC/MS data of this composition showed that its main component is 2-methyl-5-phenyl-4,5,6,7-tetrahydro-[1,2,4]triazolo[1,5-*a*]pyrimidin-7-ol MPTTP ([M+H]=231). This indicates a reaction between triazole and cinnamaldehyde under these conditions and serves as an additional explanation for the unexpected composition of the IC1.

2.3. Mass loss measurements

All electrochemical and direct corrosion experiments were carried out in an aqueous solution of 24% HCl.

Mass loss measurements were carried out in accordance with GOST 9.905-82 “Methods of corrosion testing” and GOST 9.907-83 “Methods for removing products after corrosion testing”. Corrosion tests were carried out on steel plates (20×40 mm, thickness 1.2 mm). Each sample was preliminarily polished with K1000 fine-grained sandpaper, after which it was washed with distilled water, ethanol, and dried with filter paper. The experiments were carried out in a 24% HCl solution (for 7 days) under natural aeration without stirring for three samples in parallel (for each inhibitor concentration). After testing, the plates were washed with distilled water and treated with compositions in accordance with GOST 9.907-83.

The corrosion rate was determined according to the weight loss of the samples and was calculated using the formula:

$$k_{\text{inh}} = \frac{\Delta m}{St},$$

where $\Delta m = m_0 - m$ (m_0 is the weight of the sample before the start of the experiment, m is the weight of the sample after the test, g), S is the total surface area of the plate, m^2.

For each solution, the corrosion rate k_0 without inhibitor additive was determined ($k_{0(\text{average})} \approx 16.9 \pm 0.5$ g/(m^2·hour) is the average value of the corrosion rate without addition of an inhibitor, obtained over the course of the studies). The inhibitory effect of the aminotriazole derivatives was evaluated according to the value of the inhibition coefficient:

$$\gamma = \frac{k_0}{k_{inh}},$$

and the degree of protection:

$$Z_k = \frac{(k_0 - k_{inh})}{k_0} \cdot 100\%,$$

where k_0 and k_{inh} are the corrosion rates in the background solution and in the solution with the inhibitor, respectively.

2.4. Potentiodynamic polarization measurements

Polarization curves were obtained on an electrode made of St3 steel (with an area of 1.0 cm^2) in a three-electrode electrochemical cell with undivided electrode spaces using an IPC-Pro potentiostat (Frumkin Institute of Physical Chemistry and Electrochemistry Russian Academy of Sciences). The working electrode was preliminarily cleaned with K2000 sandpaper (5.2–6.2 μm grit) and degreased with ethyl alcohol. The electrode potential (E) was measured relative to the silver chloride electrode by connecting the space of the electrochemical cell and the reference electrode (its potential is +202 mV relative to the standard hydrogen electrode) *via* an electrolytic bridge based on agar-agar and $NaNO_3$. A platinum grid was used as an auxiliary electrode. The potential values are given on the scale of a standard hydrogen electrode.

The substances were introduced into the acid until the required concentration was obtained. The electrodes were immersed in the solution and kept for 30 minutes, until the free corrosion potential (E_{cor}) was established. Next, potentiodynamic polarization curves were obtained at 0.2 mV/s in the anodic and cathodic directions from the value of E_{cor}. Polarization curves were recorded until the current density i reached ±0.1 $A \cdot cm^{-2}$.

The corrosion rate in current units was determined by the polarization resistance technique as summarized by Mansfeld [20]. Electrodes and a cell were prepared for this as described above. After E_{cor} was established, the electrode was polarized in the range of ±30 mV from the E_{cor} value in the potentiodynamic mode at a scanning rate of 0.2 mV/s.

Polarization resistance R_p was determined as a slope of the polarization curve at E_{cor} in the coordinates $\Delta E–i$, where ΔE is the difference between the electrode potential and the open-circuit potential ($E–E_{cor}$). Next, the graph was plotted with the coordinates $2.3 \cdot R_p \cdot i–\Delta E$. The coefficients b_a and b_c, *i.e.* the Tafel slopes of the cathodic and anodic segments of the polarization curve) were determined using the Table Curve2D soft as the approximation parameters of the equation:

$$2.3 \cdot R_p \cdot I = \frac{b_a \cdot b_c}{b_a + b_c}\left[\exp\left(\frac{E - E_{cor}}{b_a}\right) - \exp\left(-\frac{E - E_{cor}}{b_c}\right)\right].$$

The corrosion current was calculated taking into account the coefficients obtained according to the equation:

$$I_{cor} = \frac{B}{R_p}.$$

The corrosion current density (i_{cor}) was calculated as follows:

$$i_{cor} = \frac{I_{cor}}{S}.$$

Based on the results of potentiodynamic measurements, the inhibitor efficiency was estimated as the ratio of i_{cor} for each concentration of the studied substances to the current density of the blank experiment ($i_{cor,0}$=6.8 mA/cm^2):

$$i_{cor(relative)} = \frac{i_{cor}}{i_{cor}^0} \cdot 100\%.$$

Measurements for each concentration of the substance were made at least 5 times until reproducible data were obtained with subsequent statistical processing of the experimental data.

2.5. Electrochemical Impedance Spectroscopy (EIS)

The electrode and all the solutions were prepared similarly to section 2.4. The EIS spectra were recorded using an IPC-Pro potentiostat and an FRA-2 attachment for frequency response analysis. After E_{cor} was established, the frequency dependence was recorded in the range from 0.01 to 50.000 Hz in the open-circuit mode (at E_{cor}). The frequency dependence analysis, the selection of an equivalent circuit, and the determination of the nominal values of its components were performed using the DCS software package supplied with the FRA-2 analyzer.

2.6. Scanning electron microscopy (SEM)

For microscopic analysis of the surface, a Jeol JSM-680LV raster electron microscope (Japan) was used together with Oxford Instrument INCA 250 X-ray microanalysis module (UK) which determines the chemical composition of the surface layer. The research results were obtained on the equipment of the collective use Center of Voronezh state University (http://ckp.vsu.ru).

The electrodes were prepared as described above and immersed in the appropriate acid solutions without any additives or with the addition of the test substances or compositions. After exposure for 1 hour, the electrodes were removed from the solution, washed with distilled water, and dried in a kiln at 80°C.

2.7. Quantum-chemical calculations

All the synthesized molecules and their isomeric (tautomeric form) forms are fully optimized using density functional theory (DFT) with B3LYP functional using 6-311+G (d,p) basis set in Gaussian program [21]. The optimized geometries are showing non-negative frequencies

which results in molecules are located at minimum energy in potential energy surface. The determination of *HOMO*, *LUMO* energies, HOMO-LUMO gap (*HLG*), as well as the ionization potential (*IP*), electron affinity (*EA*), electronegativity (χ), absolute hardness (η) and softness (σ) for all the molecules were carried out at same level of theory.

From density functional theory the absolute hardness (η) is defined as [22]

$$\eta = \frac{1}{2}\frac{\partial \mu}{\partial N} = \frac{1}{2}\frac{\partial^2 E}{\partial N^2},$$

where μ is chemical potential and N is the number of electron and E is the energy. R.G. Pearson proposed an operational definition for absolute hardness as

$$\eta = \frac{IP - EA}{2}.$$

Also from Koopman's theorem, from an orbital basis *IP* and *EA* are defined as

$$IP = -E_{\mathrm{HOMO}}; EA = -E_{\mathrm{LUMO}}$$

where E_{HOMO} and E_{LUMO} are the energies of highest occupied and lowest unoccupied molecular orbitals.

Electronegativity (χ) is also defined in terms of *HOMO* and *LUMO* energies as

$$\chi = \frac{IP + EA}{2}.$$

From the above formulas, hardness is a measure of the resistance to any changes in the electron cloud of a chemical systems, it is also an important parameter in the field of reaction chemistry. Absolute softness (σ) is inversely proportional to hardness.

It is known that the most reactive homologues in the series of organic compounds have a higher softness value [22]. In addition, the ability of inhibitors to interact with the metal surface increases with an increase in the *HOMO* energy and a decrease in the *LUMO* energy. The smaller *HLG*, the higher the reactivity of the inhibitor to the metal surface, and the stronger the inhibitory effect.

All these notions make it possible to theoretically evaluate and compare the degree of interaction of inhibitors with a metal and, as a result, to predict their probable inhibitive properties.

3. Results and Discussion

3.1. Mass loss measurements

At the first stage, the study of corrosion inhibition of the substances was carried out by gravimetric (mass loss) measurements. The results obtained in this way can be directly used in practice without additional complicated processing. The measurements were repeated at least 3 times. For all studied substances and compositions in concentrations (C_{inh}) from 0.10 to 2.00 $\mathrm{g \cdot dm^{-3}}$ the inhibition coefficients were at least 1.84 (Table 4). Protection degree (Z)

increases with increasing concentration of substances. The exception was IC1, for which a slight decrease in protection values is found when going from 0.10 to 0.50 $g \cdot dm^{-3}$. The highest *Z* values for the individual substances ATCA and MPTTP were 74.43% and 78.55%, respectively. These values are achieved at $C_{inh} \approx 0.10\ g \cdot dm^{-3}$ for ATCA and $2.00\ g \cdot dm^{-3}$ for MPTTP. Any results for higher concentrations of ATCA could not be obtained due to limited solubility.

Compositions based on these substances showed significantly higher values of the protection degree, not less than 93%. The highest degree of protection (97.47%) was obtained for IC1 at $C_{inh} = 2.00\ g \cdot dm^{-3}$. For IC2, the maximum degree of protection was 95.57% at $C_{inh} = 2.00\ g \cdot dm^{-3}$ and remained almost unchanged at $C_{inh} = 1.00\ g \cdot dm^{-3}$.

Table 4. Results of the weight loss measurements of mild steel plates in 24% HCl solutions with various inhibitors.

Inhibitor	Concentration of inhibitor, C_{inh}, $g \cdot dm^{-3}$	Corrosion rate, k, $g \cdot m^2 \cdot hour^{-1}$	Inhibition coefficient, γ, %	Protection degree, *Z*, %
None	–	16.90	–	–
ATCA	~0.10	4.32	3.91	74.43
MPTTP	0.10	9.19	1.84	45.61
	0.50	7.29	2.32	56.84
	1.00	7.24	2.33	57.12
	2.00	3.62	4.66	78.55
IC1	0.10	0.94	17.95	94.43
	0.50	1.15	14.58	93.14
	1.00	0.77	21.79	95.41
	2.00	0.42	39.53	97.47
IC2	0.10	1.16	14.58	93.14
	0.50	0.99	17.12	94.16
	1.00	0.79	21.46	95.34
	2.00	0.75	22.57	95.57

3.2. Potentiodynamic polarization measurements

At the next stage, potentiodynamic measurements were carried out to obtain complete anodic and cathodic polarization curves and estimate the corrosion current density (i_{cor}) in an HCl solution with additives of substances at concentrations similar to paragraph 3.1.

The addition of ATCA at $C_{inh} \approx 0.10\ g \cdot dm^{-3}$ leads to a slight (up to 13 mV) shift of E_{cor} in the positive direction (Table 5) and is accompanied by a decrease in the current density in the cathode section of the polarization curve (Figure 4a). Anodic curve sites for the control

experiment and in the presence of ATCA are indistinguishable. Thus, only a slight protective effect due to the suppression of the cathodic hydrogen reduction process can be assumed. The calculated value of i_{cor} is less than for measurement without additive, but the degree of protection does not exceed 13.2% (Table 5).

For MPTTP, a continuous shift of E_{cor} in the positive direction is observed with increasing concentration. The maximum difference was obtained at C_{inh}≈2.00 g·dm^{-3} and it is +56 mV. The current density in the anodic and cathodic segments of the polarization curves decreases with increasing C_{inh} relative to the blank experiment (Figure 4b). This indicates an increase in the inhibitive effect. Thus, the cathodic and anodic partial processes are suppressed [23]. The degree of protection increases from 64.7% to 95.4% in the studied concentration range.

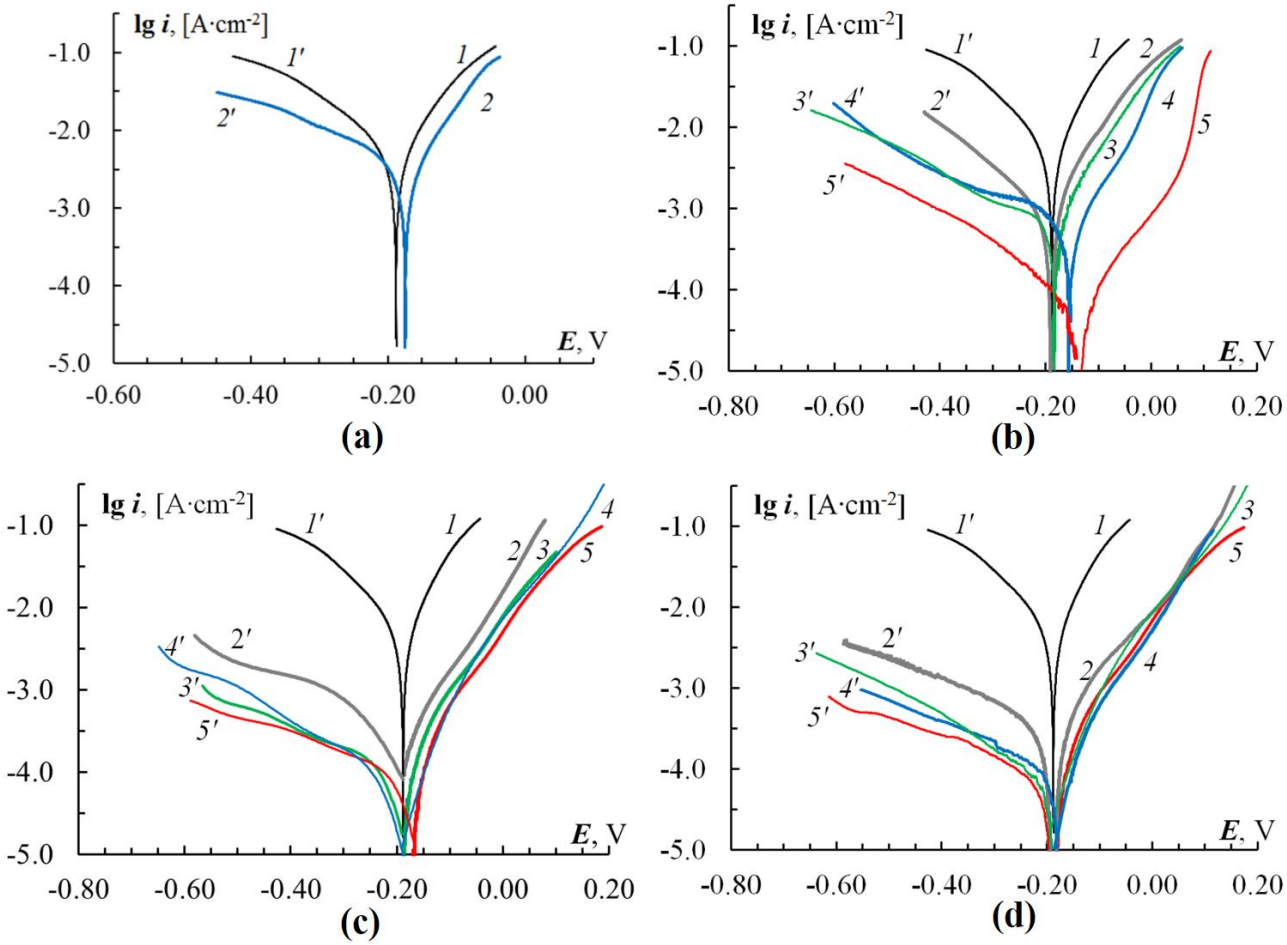

Figure 4. Anodic (1–5) and cathodic (1′–5′) polarization curves of mild steel electrode in 24% HCl solutions and ATCA (a), MPTTP (b), IC1 (c) and IC2 (d) at C_{inh}, g·dm^{-3}: 1, 1′ – 0.00; 2, 2′ – 0.10; 3, 3′ – 0.50; 4, 4′ – 1.00; 5, 5′ – 2.00.

E_{cor} was only slightly different from the blank experiment when compositions IC1 or IC2 were added into the acidic solution. With an increase in C_{inh} of IC1, a decrease in current densities in the anodic and cathodic sections of the polarization curves was noted (Figure 4c).

In this case, the relative decrease in the cathode sections was more pronounced. In this case, the relative decrease for the cathodic sections was more significant. In this regard, a mixed mechanism of inhibition with a predominance of the cathodic process can be assumed. The highest degree of protection was obtained at C_{inh}=2.00 g·dm^{-3} and amounted to 98.1%. For IC2, the nature of the change in the polarization curves was close to that of IC1 (Figure 4d). The degree of protection was also >98%.

Thus, the anticorrosive properties obtained on the basis of both weight-loss and potentiodynamic measurements showed the same trends. Mixed inhibitory compositions had a higher inhibitive effect compared with the individual substances ATCA and MPTTP. The observed difference between the protection degrees obtained by weight-loss and potentiodynamic methods is most likely due to the different duration of the experiments. The weight-loss experiments gave an average corrosion rate over a period of 7 days, while the electrochemical determination of the corrosion rate was made immediately half an hour after the electrode was immersed in the solution.

Table 5. Electrochemical characteristics of mild steel electrode in 24% HCl solutions with corresponding inhibitors.

Inhibitor	**Concentration of inhibitor, C_{inh}, g·dm^{-3}**	**Open circuit potential, E_{cor}, V**	**Polarization resistance, R_p, Ω·cm^2**	**Corrosion current density, i_{cor}, mA·cm^{-2}**	**Protection degree, Z_i, %**
without	–	–0.191±0.006	4.2±0.5	6.80±0.30	–
ATCA	≈0.10	–0.178±0.002	5.1±0.3	5.90±1.20	13.2
MPTTP	0.10	–0.188±0.012	16.1±1.2	2.40±0.30	64.7
	0.50	–0.180±0.009	43.0±4	1.10±0.15	83.8
	1.00	–0.160±0.014	47.0±3	1.03±0.19	84.9
	2.00	–0.135±0.006	134.0±18	0.28±0.06	95.9
IC1	0.10	–0.187±0.013	58.0±7	0.84±0.07	87.6
	0.50	–0.190±0.017	63.0±9	0.56±0.09	91.7
	1.00	–0.190±0.008	141.0±16	0.31±0.05	95.4
	2.00	–0.169±0.009	269.0±24	0.13±0.03	98.1
IC2	0.10	–0.193±0.012	38.0±6	1.15±0.14	83.1
	0.50	–0.186±0.008	115.0±11	0.36±0.06	94.7
	1.00	–0.186±0.010	152.0±18	0.15±0.03	97.8
	2.00	–0.175±0.004	296.0±13	0.11±0.02	98.1

3.3. Electrochemical impedance spectroscopy (EIS)

Electrochemical impedance spectroscopy was used to confirm the results of potentiodynamic measurements and to obtain additional information about the mechanism of the protective action of the analyzed substances and compositions. Analyzing the obtained results for MPTTP, we used the Mansfeld equivalent circuit (Figure 5a). In all other cases, when the Nyquist plots had a simpler form that has been widely described in the literature, a simplified circuit (Figure 5b) was used [24–26].

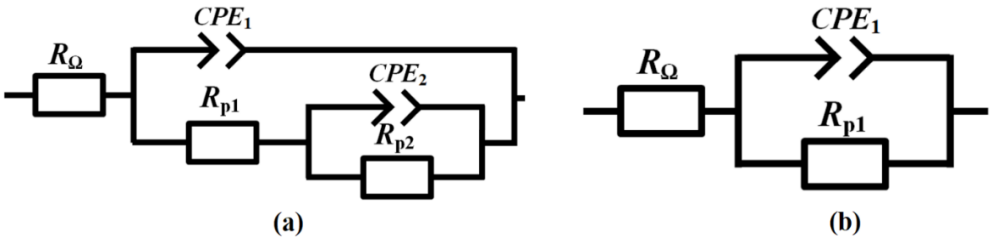

Figure 5. An equivalent Mansfeld circuit (a) and a simplified version (b) for describing the experimental results of EIS for the studied inhibitors (R_Ω – ohmic resistance, CPE_1, CPE_2 – constant phase element of the electrochemical reaction No. 1 and 2; R_{p1}, R_{p2} – polarization resistance of the electrochemical reaction N 1 and 2).

The Nyquist plot for the blank measurement without any additives (Figure 6a,1) had the shape of a deformed semicircle. The diameter of the semicircles increased in the comparison to the blank experiment with the addition of ATCA (Figure 6a), IC1 (Figure 6c), and IC2 (Figure 6d), as well as with concentration increasing of each additive. The Nyquist plots in the solution with addition of MPTTP (Figure 6b) consisted of two semicircles.

The low-frequency semicircles for all measurements were strongly flattened. It is assumed that a certain layer was formed on the electrode surface, which increases the resistance R_{p1} with increasing concentration. This layer created an obstacle to the electrochemical process in the low-frequency region, the resistance of which R_{p2} is also increased with increasing concentration. The simplification of the secondary semicircle (Figure 6b) was probably caused by the diffuse structure of the electric double layer. Such a process can occur, for example, in the pores of the adsorption layer.

The inhibition efficiency (η_{inh}) was calculated by comparing the R_p values for the blank experiment and in the presence of the additive as follows:

$$\eta_{inh} = \left(1 - \frac{R_{p(blank)}}{R_p}\right) \cdot 100 .$$

In case of the Mansfeld circuit, R_p was taken as the sum ($R_{p1} + R_{p2}$).

The values of the EIS equivalent circuit elements of a steel electrode in 24% HCl solution without additive and in the presence of various concentrations of inhibitors are presented in Table 6. The results obtained are consistent with the proposed protection mechanism.

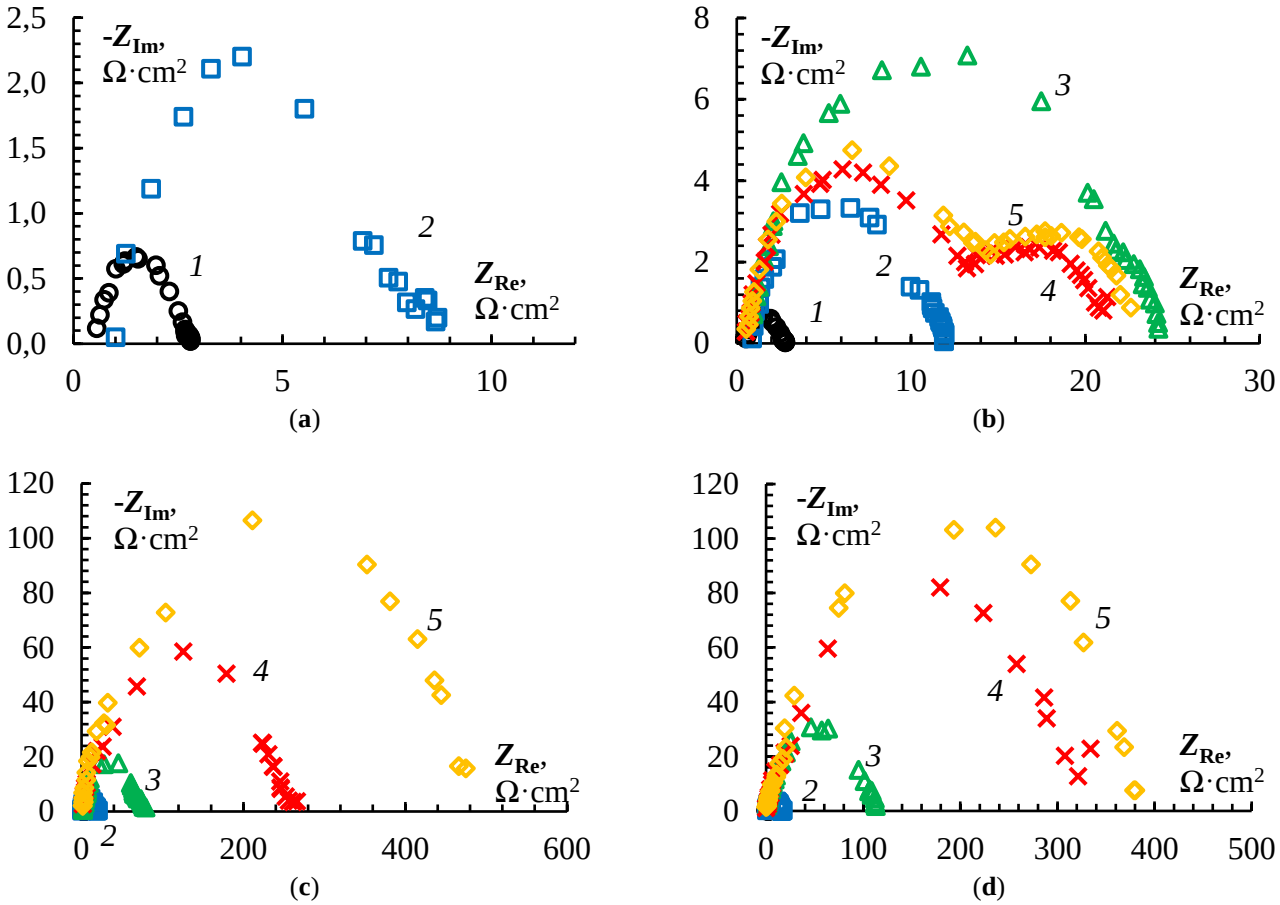

Figure 6. The Nyquist diagrams of mild steel electrode in 24% HCl solutions in the presence ATCA (a), MPTTP (b), IC1 (c) and IC2 (d) at C_{inh}, g·dm^{-3}: 0.10 (2), 0.50 (3), 1.00 (4) and 2.00 (5) (without an inhibitor – 1).

Table 6. Equivalent circuit elements and degree of protection of mild steel electrode in 24% HCl solutions with different inhibitors.

Inhibitor	Concentration of inhibitor, C_{inh}, g/dm^3	Ohmic resistance, R_Ω, Ω·cm^2	Polarization resistance, R_{p1}, Ω·cm^2	CPE$_1$, μF·cm^{-2}	n_1	Polarization resistance, R_{p2}, Ω·cm^2	CPE_2, μF·cm^{-2}	n_2	Degree of protection η_i, %
None	–	0.41±0.03	2.33±0.01	0.0032±0.0003	0.636±0.012	–	–	–	–
ATCA	~0.1	0.93±0.08	7.1±0.3	0.0018±0.0008	0.66±0.06	–	–	–	67.2
MPTTP	0.1	0.91±0.04	2.7±0.3	0.00052±0.00003	1.000	7.8±0.8	0.0062±0.0004	0.44±0.02	77.7
	0.5	0.93±0.08	12.6±0.4	0.00039±0.00009	1.000	8.9±0.9	0.0052±0.0005	0.75±0.02	89.2
	1.0	0.58±0.03	14.4±0.5	0.00011±0.00002	0.87±0.01	10.4±1.5	0.027±0.004	0.55±0.02	89.3
	2.0	0.45±0.06	19.7±1.6	0.00014±0.00002	0.83±0.01	17.4±1.6	0.041±0.005	0.59±0.02	93.7
IC1	0.1	0.28±0.04	26±6	0.00061±0.00008	0.672±0.009	–	–	–	91.0
	0.5	0.53±0.04	76±3	0.00029±0.00002	0.656±0.003	–	–	–	96.9
	1.0	0.22±0.03	276±26	0.00021±0.00005	0.60±0.03	–	–	–	99.2
	2.0	0.20±0.02	446±18	0.00022±0.00002	0.576±0.015	–	–	–	99.5
IC2	0.1	0.78±0.08	16±2	0.00066±0.00009	0.697±0.015	–	–	–	85.4
	0.5	0.40±0.03	110±3	0.00018±0.00004	0.644±0.015	–	–	–	97.9
	1.0	0.34±0.05	402±31	0.00021±0.00004	0.59±0.02	–	–	–	99.4
	2.0	0.20±0.01	410±16	0.00014±0.00002	0.633±0.004	–	–	–	99.4

In the presence of ATCA, the protective effect was 67.2%. For MPTTP, an increase in the degree of protection from 77.7 to 93.7% was observed with increasing concentrations in the studied concentration range. Compositions IC1 and IC2 showed higher protective properties, reaching values of the protection degree of 99.4–99.5% at C_{inh}=2.00 g/dm^{-3} according to the results of potentiodynamic measurements, similar to the direct weight loss measurements. In general, the EIS results more closely matched the results of the direct gravimetric corrosion tests described above.

3.4. Scanning electron microscopy (SEM)

The SEM method was used to obtain microphotographs of the electrode surfaces after its exposure in the HCl solution without any additives and in the presence of the studied substances and compositions.

After the electrode was exposed in the HCl solution without additives, a developed structure with peaks and troughs up to 10 μm in size was formed on the steel surface (Figure 7a). The addition of ATCA $C_{inh}\approx$0.10 g·dm^{-3} reduced the peak sizes, but traces of steel dissolution were present on the surface to the point where grooves from sanding paper were not identified (Figure 7b).

When the substances MPTTP, IC1 and IC2 (C_{inh}=1.00 and 2.00 g·dm^{-3}) are added to the solution, the appearance of the electrode surface practically does not change compared to the initial state of the surface (Figure 7 c–h): grooves from sanding paper are clearly visible.

The 3−5 μm pits found on the microphotographs are not the result of corrosion processes that have occurred, but were present on the analyzed surfaces before the start of pickling. This result fully correlates with the data of polarization measurements, impedance spectroscopy, and direct corrosion tests. It shows the significant effectiveness of the developed steel acid corrosion inhibitors.

The composition of the surface layer in the above pictured areas are presented in Table 7. All electrodes after exposure in the HCl solution showed Fe fraction decreased from 92.80% to 57.71%−79.15%. No chlorine was detected on the electrode surface without an inhibitor. In the presence of inhibitors (except for IC2 C_{inh}=1.00 g·dm^{-3}), the film had an insignificant inclusion of Cl atoms in an amount from 0.30% to 1.06%. An increase in the amount of C and O atoms was also found after exposure in acid solutions. The correlation between the protection degree and the changes in the proportion of elements composition detected on the steel surfaces has not been established. Nitrogen atoms were not detected, which suggests that the molecules of the studied substances were removed during the washing and drying of the electrodes before the X-ray microanalysis.

Table 7. Elemental surface composition (at. %) of the mild steel electrode.

Exposure conditions	Element				
	Fe	**C**	**O**	**Mn**	**Cl**
before exposure	92.80	6.00	0.60	0.33	–
after exposure without inhibitor	75.19	20.92	3.52	0.37	–
after exposure with ATCA, $C_{inh} \approx 0.10$ g·dm^{-3}	62.54	20.70	15.59	0.36	0.81
after exposure with MPTTP, $C_{inh} = 1.00$ g·dm^{-3}	77.00	9.55	12.23	0.32	0.30
after exposure with MPTTP, $C_{inh} = 2.00$ g·dm^{-3}	79.15	5.18	14.87	0.46	0.46
after exposure with IC1, $C_{inh} = 1.00$ g·dm^{-3}	67.23	22.65	10.17	0.20	0.25
after exposure with IC1, $C_{inh} = 2.00$ g·dm^{-3}	70.03	14.71	13.98	0.22	1.06
after exposure with IC2, $C_{inh} = 1.00$ g·dm^{-3}	62.19	33.65	3.96	0.20	–
after exposure with IC2, $C_{inh} = 2.00$ g·dm^{-3}	57.71	30.85	10.67	0.30	0.47

3.5. Quantum-chemical calculations

Calculation results of *HOMO*, *LUMO*, HOMO-LUMO (*HLG*) energies, ionization potential (*IP*), electron affinity (*EA*), electronegativity (χ), absolute hardness (η) and softness (σ) for the studied individual substances ATCA and MPTTP are shown in Table 8.

Table 8. Optimized structures, calculated *HOMO*, *LUMO* energies, HOMO-LUMO gap (*HLG*), Ionization Potential (*IP*), Electron Affinity (*EA*), Electronegativity (χ), Absolute Hardness (η) and Softness (σ) in eV at B3LYP/6-311+G (d,p) level of theory.

Inhibitor	***HOMO***	***LUMO***	***HLG***	***IP***	***EA***	**χ**	**η**	**σ**
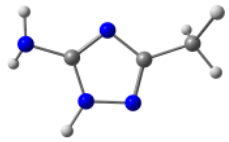 ATCA	–6.432	–0.501	5.930	6.435	0.509	3.468	2.968	0.341
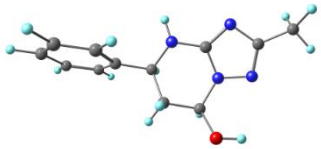 MPTTP	–6.207	–0.898	5.309	6.207	0.898	3.553	2.655	0.377

For 2-alkyl-5-phenyl-4,5,6,7-tetrahydro-[1,2,4]triazolo[1,5-*a*]pyrimidin-7-ols, a decrease in the *HLG* value, an increase in the absolute softness of the inhibitor molecule, an increase in electron affinity are observed in comparison with 3-alkyl-5-amino-1*H*-1,2,4-triazoles. That is, all the theoretical signs of improving the ability of the inhibitor molecule

to form bonds with the metal and increase the anticorrosive properties are observed. These results are in good agreement with the obtained experimental data.

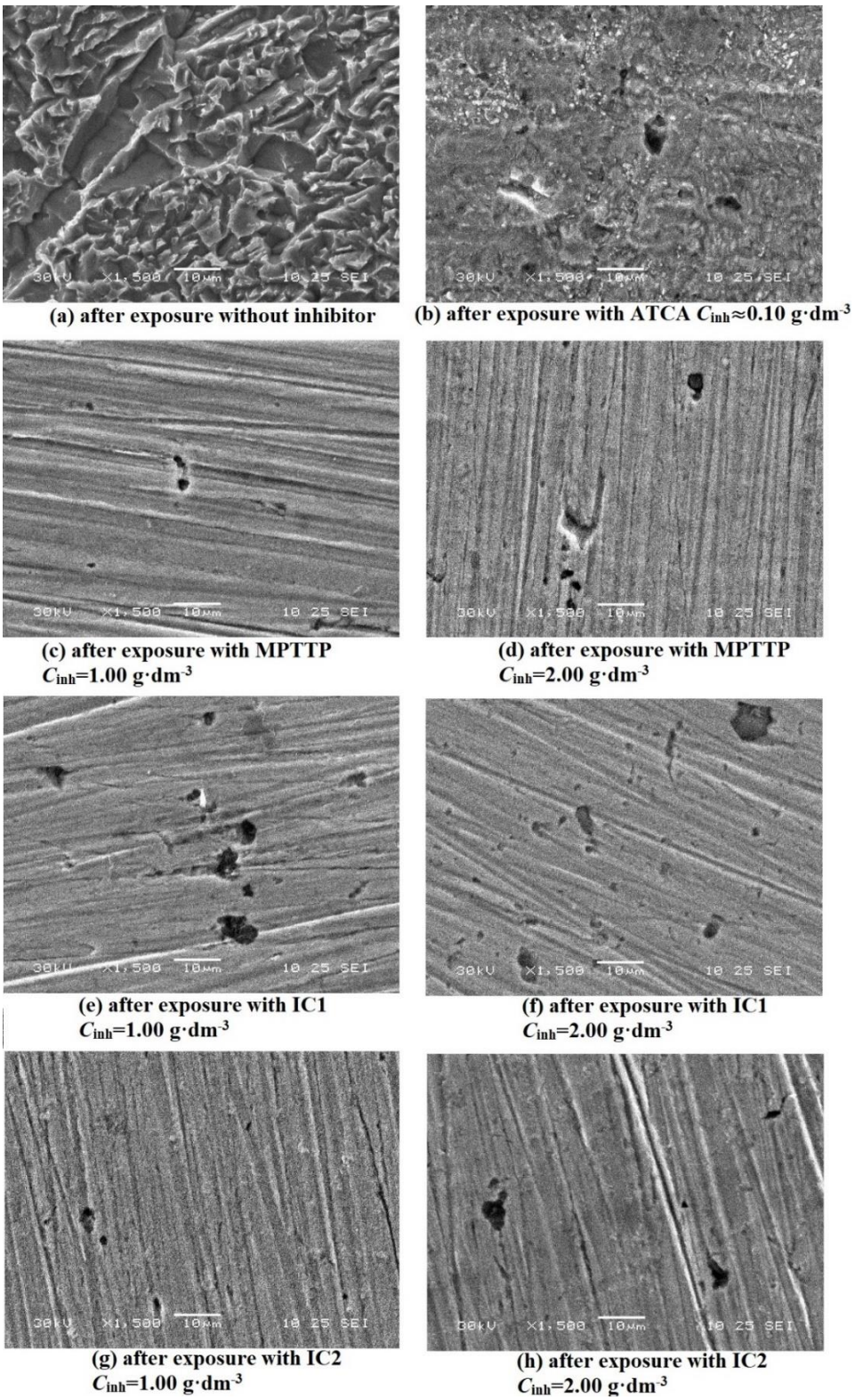

Figure 7. SEM micrographs of mild steel surface at ×1500 magnification (the captions are provided under the images).

It should be noted that in our earlier studies on the anticorrosion effect of 3-alkyl-5-amino-1*H*-1,2,4-triazoles derivatives [27], it was shown that such substances have a low inhibition effect on steel corrosion in acidic solutions. Besides, we also showed that triazole mixtures based on vegetable oil processing wastes are also not highly effective inhibitors of hydrochloric acid corrosion of low-carbon steel and have a solubility of no more than 0.10 $g \cdot dm^{-3}$. On the other hand, in this article, based on our recent experiments, it is shown that individually synthesized 2-methyl-5-phenyl-4,5,6,7-tetrahydro-[1,2,4]triazolo[1,5-*a*]pyrimidine-7-ol MPTTP, as well as both developed compositions of inhibitors (IC1, IC2) are much more soluble in hydrochloric acid, and also exhibit significantly higher protective properties compared to the ATCA mixture.

4. Conclusions

A complex of full-scale, electrochemical, and physical methods showed a high protective effect of the synthesized compound (MPTTP) and a mixture of aminotriazoles ATCA, as well as compositions based on them (IC1, IC2) with the addition of cocamidopropyl betaine and cinnamic aldehyde in relation to low-carbon steel in solution 24 % HCl.

The high protective effect found for the developed compositions is probably associated with the reaction of aminotriazoles with cinnamaldehyde during the preparation of the inhibitive compositions. Such reaction results in the formation of the corresponding derivatives of the 2-alkyl-5-phenyl-4,5,6,7-tetrahydro-[1,2,4]triazolo[1,5-*a*]pyrimidin-7-ol class similarly to the formation of MPTTP.

The synthesized MPTTP was found to have a high protection degree of at least 93% at the concentration of 2.00 $g \cdot dm^{-3}$. This additionally explains the high protective effect of the IC1, IC2 compositions, which, accordingly to HPLC/MS data, also contain derivatives of the tetrahydro-[1,2,4]triazolo[1,5-*a*]pyrimidin-7-ol class.

IC1 composition, obtained using an amphoteric surfactant – cocamidopropyl betaine, cinnamaldehyde and a mixture of aminotriazoles ATCA, was the most effective among the other substances in inhibiting acid corrosion of mild steel. Its protection degree was at least 95% at the concentration of at least 0.50 $g \cdot dm^{-3}$, while the corrosion rate was 0.4−1.0 $g/m^2 \cdot hour$.

The chemical modification of alkylaminotriazole molecules by their condensation with cinnamaldehyde makes it possible to obtain a fundamentally new class of highly effective steel acid corrosion inhibitors – 5-aryl-4,5,6,7-tetrahydro-[1,2,4]triazolo[1,5-*a*] pyrimidin-7-ols. Moreover, along with a high inhibitory activity, these substances have a high solubility in HCl, which makes it possible to obtain homogeneous solutions of inhibited mineral acids based on them. This opens up broad prospects for the convenient use of such derivatives at real industrial facilities.

Acknowledgements

The study was supported by the Russian Science Foundation (RSF), project No. 22-23-01144, https://rscf.ru/en/project/22-23-01144/.

References

1. C.N. Fredd and H.S. Fogler, Alternative stimulation fluids and their impact on carbonate acidizing, *SPE Formation Damage Control Symposium*, 1996. doi: 10.2118/31074-MS
2. E. Barmatov, J. Geddes, T. Hughes and M. Nagl, Research on corrosion inhibitors for acid stimulation, *Corrosion*, 2012.
3. A.G. Gad Allah and H. Moustafa, Quantum mechanical calculations of amino pyrazole derivatives as corrosion inhibitors for zinc, copper and α-brass in acid chloride solution, *J. Appl. Electrochem*., 1992, **22**, no. 7, 644–648. doi: 10.1007/BF01092613
4. S.I. Mostafa and S.A. Abd El-Maksoud, Synthesis and characterization of some transition metal complexes of 2-amino-3-hydroxypyridine and its application in corrosion inhibition, *Monatsh. Chem*., 1998, **129**, no. 5, 455–466. doi: 10.1007/PL00000102
5. L.S. Nandeesh and B.S. Sheshadri, Inhibitory effect of 2-mercapto pyrimidine on corrosion of copper single crystal planes in 0.1 M H_2SO_4, *Proc. Indian Acad. Sci. – Chem. Sci*., 1991, **103**, no. 6, 763–775. doi: doi: 10.1007/BF02867330
6. U. Habib, A. Badshah, Ul. Flörke, R.A. Qureshi, B. Mirza, Nazar-ul-Islam and A. Khan, Synthesis of (2,4-diamino-5-(3′,4′,5′-trimethoxybenzyl) pyrimidine) copper (II) complex at 20-25°C and its structural characterization, *J. Chem. Crystallogr*., 2009, **39**, no. 8, 607–611. doi: 10.1007/s10870-009-9547-7
7. S. Zor, Sulfathiazole as potential corrosion inhibitor for copper in 0.1 M NaCl, *Prot. Met. Phys. Chem. Surf*., 2014, **50**, no. 4, 530–537. doi: 10.1134/S2070205114040200
8. L.H. Madkour and I.H. Elshamy, Experimental and computational studies on the inhibition performances of benzimidazole and its derivatives for the corrosion of copper in nitric acid, *Int. J. Ind. Chem*., 2016, **7**, no. 2, 195–221. doi: 10.1007/s40090-015-0070-8
9. D.Q. Zhang, L.X. Gao and G.D. Zhou, Synergistic effect of 2-mercapto benzimidazole and KI on copper corrosion inhibition in aerated sulfuric acid solution, *J. Appl. Electrochem*., 2003, **33**, no. 5, 361–366. doi: 10.1023/A:1024403314993
10. M. Finšgar and I. Milosev, Inhibition of copper corrosion by 1,2,3-benzotriazole: A review, *Corros. Sci*., 2010, **52**, no. 9, 2737–2749. doi: 10.1016/j.corsci.2010.05.002
11. Yu.I. Kuznetsov, M.O. Agafonkina, Kh.S. Shikhaliev, N.P. Andreeva and A.Yu. Potapov, Adsorption and passivation of copper by triazoles in neutral aqueous solution, *Int. J. Corros. Scale Inhib*., 2014, **3**, no. 2, 137–148. doi: 10.17675/2305-6894-2014-3-2-137-148
12. Z. Khiati, A.A. Othman, M. Sanchez-Moreno, M.C. Bernard, S. Joiret, E.M.M. Sutter and V. Vivier, Corrosion inhibition of copper in neutral chloride media by a novel derivative of 1,2,4-triazole, *Corros. Sci*., 2011, **53**, no. 10, 3092–3099. doi: 10.1016/j.corsci.2011.05.042

13. E. Stupnišek-Lisac, A. Gazivoda and M. Madžarac, Evaluation of non-toxic corrosion inhibitors for copper in sulphuric acid, *Electrochim. Acta*, 2002, **47**, no. 26, 4189–4194. doi: 10.1016/S0013-4686(02)00436-X
14. M.A. Quraishi and D. Jamal, Fatty acid triazoles: Novel corrosion inhibitors for oil well steel (N-80) and mild steel, *J. Am. Oil Chem. Soc*., 2000, **77**, no. 10, 1107–1111. doi: 10.1007/s11746-000-0174-6
15. D. Graiver, R. Dacomba, M. Khawaji, A. Jaros, K. Berglund and R. Narayan, Steel-corrosion inhibitors derived from soybean oil, *J. Am. Oil Chem. Soc*., 2012, **89**, no. 10, 1895–1903. doi: 10.1007/s11746-012-2077-z
16. I.A. Aiad, A.A. Hafiz, M.Y. El-Awady and A.O. Habib, Some imidazoline derivatives as corrosion inhibitors, *J. Surfactants Deterg*., 2010, **13**, no. 3, 247–254. doi: 10.1007/s11743-009-1168-9
17. M.A. Quraishi, D. Jamal and M.T. Saeed, Fatty acid derivatives as corrosion inhibitors for mild steel and oil-well tubular steel in 15% boiling hydrochloric acid, *J. Am. Oil Chem. Soc*., 2000, **77**, no. 3, 265–268. doi: 10.1007/s11746-000-0043-3
18. T.B. Gaines, R.D. Kimbrough and R.E. Linder, The toxicity of amitrole in the rat, *Toxicol. Appl. Pharmacol*., 1973, **26**, no. 1, 118–129. doi: 10.1016/0041-008x(73)90092-6
19. D.S. Shevtsov, Kh.S. Shikhaliev, N.V. Stolpovskaya, A.A. Kruzhilin, A.Yu. Potapov, I.D. Zartsyn, O.A. Kozaderov, D.V. Lyapun, C. Prabhakar and A. Tripathi, 3-Alkyl-5-amino-1,2,4-triazoles synthesized from the fatty acids of sunflower oil processing waste as corrosion inhibitors for copper in chloride environments, *Int. J. Corros. Scale Inhib*., 2020, **9**, no. 2, 726–744. doi: 10.17675/2305-6894-2020-9-2-21
20. F. Mansfeld, Tafel slopes and corrosion rates obtained in the pre-Tafel region of polarization curves, *Corros. Sci*., 2005, **47**, no. 12, 3178–3186. doi: 10.1016/j.corsci.2005.04.012
21. M.J. Frisch, G.W. Trucks, H.B. Schlegel, G.E. Scuseria, M.A. Robb, J.R. Cheeseman, G. Scalmani, V. Barone, G.A. Petersson and H. Nakatsuji, Gaussian16 Revision B.01, Gaussian Inc. Wallingford CT, 2016. https://gaussian.com/g16main
22. R.G. Parr and R.G. Pearson, Absolute hardness: companion parameter to absolute electronegativity, *J. Am. Oil Chem. Soc*., 1983, **105**, no. 26, 7512–7516. doi: 10.1021/ja00364a005
23. A. Farhadian, S.A. Kashani, A. Rahimi, E.E. Oguzie, A.A. Javidparvar, S.C. Nwanonenyi, S. Yousefzadeh and M.R. Nabid, Modified hydroxyethyl cellulose as a highly efficient eco-friendly inhibitor for suppression of mild steel corrosion in a 15% HCl solution at elevated temperatures, *J. Mol. Liq*., 2021, **338**, 116607. doi: 10.1016/j.molliq.2021.116607
24. H.A. Al-Sharabi, F. Bouhlal, K. Bouiti, N. Labjar, E.Al Zalaei, A. Dahrouch, G.A. Benabdellah, M.El Mahi, B. Benmessaoud, E.M. Lotfi, B.El Otmani and S.El Hajjaji, Electrochemical and thermodynamic evaluation on corrosion inhibition of

C38 steel in 1 M HCl by Rumex ethanolic extract, *Int. J. Corros. Scale Inhib*., 2022, **11**, no. 1, 382–401. doi: 10.17675/2305-6894-2022-11-1-23

25. L. Toukal, D.E. Belfennache, M. Foudia, R. Yekhlef, F. Benghanem, B. Hafez, H. Elmsellem and I. Abdel-Rahman, Inhibitory power of *N*,*N*′-(1,4-phenylene)bis(1-(4-nitrophenyl) methanimine) and the effect of the addition of potassium iodide on the corrosion inhibition of XC70 steel in HCl medium: Theoretical and experimental studies, *Int. J. Corros. Scale Inhib*., 2022, **11**, no. 1, 438–464. doi: 10.17675/2305-6894-2022-11-1-26
26. V. Saraswat, R. Kumari and M. Yadav, Novel carbon dots as efficient green corrosion inhibitor for mild steel in HCl solution: Electrochemical, gravimetric and XPS studies, *J. Phys. Chem. Solids*, 2022, **160**, 110341. doi: 10.1016/j.jpcs.2021.110341
27. D.V. Lyapun, A.A. Kruzhilin, D.S. Shevtsov, Yu.V. Aseeva and Kh.S. Shikhaliev, Corrosion inhibition of steel by selected homologues of the class 3-alkyl-5-amino-1*H*-1,2,4-triazoles in acidic media, *Kondens. Sredy Mezhfaznye Granitsy*, 2022, **24**, no. 1, 59–68. doi: 10.17308/kcmf.2022.24/9056

♦ ♦ ♦